Monte Carlo simulation of Joule heating in bulk and strained silicon

Eric Pop[a] and Robert W. Dutton
Department of Electrical Engineering, Stanford University, Stanford, California 94305

Kenneth E. Goodson
Department of Mechanical Engineering, Stanford University, Stanford, California 94305

(Received 30 August 2004; accepted 19 January 2005; published online 16 February 2005)

This work examines the details of Joule heating in silicon with a Monte Carlo method including efficient, analytic models for the electron bands, acoustic and optical phonon dispersion. We find that a significant portion of the initially generated phonons have low group velocity, and therefore low contribution to heat transport, e.g., optical phonons or acoustic modes near the Brillouin zone edge. The generated phonon spectrum in strained silicon is different from bulk silicon at low electric fields due to band splitting and scattering selection rules which favor *g*-type and reduce *f*-type phonon emission. However, heat generation is essentially the same in strained and bulk silicon at high fields, when electrons have enough energy to emit across the entire phonon spectrum despite the strain-induced band splitting. The results of this study are important for electro-thermal analysis of future silicon nanoscale devices. © *2005 American Institute of Physics*.
[DOI: 10.1063/1.1870106]

Understanding heat generation in silicon is of great physical interest and particularly relevant to the self-heating and reliability of nanoscale and thin-film transistors. Joule heating is often simulated with the classical drift-diffusion approach, as the dot product of the electric field and current density.[1–3] The heating rate can also be computed with the more sophisticated hydrodynamic approach, as a function of the electron temperature and an average energy relaxation time.[4] The field-dependent drift-diffusion approach does not account for the nonlocal nature of transport and phonon emission near strongly peaked electric field regions. The hydrodynamic approach suffers from simplifications inherent to using a single (averaged) carrier temperature and relaxation time, since scattering rates are strongly energy dependent. Neither method differentiates among electron energy exchange with the various phonon modes, nor do these methods give information regarding the frequencies of phonons emitted. Such spectral information is important because the emitted phonons travel at different velocities and have widely varying contributions to heat transport[5,6] and device self-heating.[7,8] The present work addresses these issues by using a Monte Carlo (MC) simulation method to compute detailed phonon generation rates at various electric fields, in technologically relevant doped bulk and strained silicon.

The details of the Monte Carlo implementation used in this work have been described elsewhere.[9] The electron energy bands are modeled with the analytic nonparabolic band approximation, including the six ellipsoidal conduction *X* valleys of silicon.[10] This is a good approximation for device voltages near or below the silicon band gap (1.1 eV), such as those of future nano-technologies, and it is significantly faster than the full-band MC method.[11,12] In addition, the low electron energy range means that both impact ionization (which is controlled by the band gap) and interband scattering with higher energy bands can be safely neglected (the *X*-*L* band separation in silicon is about 1.2 eV).

[a]Author to whom correspondence should be addressed; electronic mail: epop@alum.mit.edu

As in the typical analytic-band approach,[10] inelastic scattering with six types of intervalley phonons is incorporated. Three of these are of *g*-type, assisting electron scattering between valleys on the same *k* axis, and three are of *f*-type, when the scattering occurs between valleys on orthogonal axes. Intravalley scattering refers to scattering within the same conduction valley and usually involves only acoustic phonons.[13] Ionized impurity scattering is included with an efficient model which reduces the number of time-consuming small angle scattering events.[14] Electron transport in strained silicon is incorporated in the MC simulation as follows. The biaxial strain of silicon grown on a $Si_{1-x}Ge_x$ substrate removes the degeneracy of the conduction bands, lifting four of the six valleys by $\Delta E \simeq 0.67x$, where x is the Ge fraction of the substrate.[15] The in-plane conductivity effective mass of the two lower valleys is the lighter transverse mass m_t of silicon. The strain-induced energy splitting between the valleys also reduces *f*-type intervalley scattering, since the maximum available *f*-type phonon energy in silicon is only about 50 meV. For $x > 0.15$ the energy splitting is large enough to essentially suppress *f*-type scattering between the lower and upper valleys, and the strained silicon mobility enhancement is dominated by conduction via the two lower valleys with the lighter transverse mass. Figure 1 compares data reported by Ismail *et al.*[16] with our simulations for electron drift velocity over a wide range of electric fields. The simulation for strained silicon assumes no impurity concentration, while the bulk sample is doped to 10^{17} cm^{-3}. The strained silicon data of Ref. 16 were taken on modulation-doped structures, where transport is phonon limited at room temperature. Our simulations agree well with the data within MC and experimental error, over a large range of electric fields, and in both bulk and strained silicon. The scattering potentials used in the simulations have also been carefully calibrated over a wide range of temperatures.[9]

Typical MC codes treat phonon scattering with a simplified dispersion relationship, often grouping the longitudinal (LA) and transverse acoustic (TA) branches into a dispersionless mode with constant group velocity,[10] and assuming a

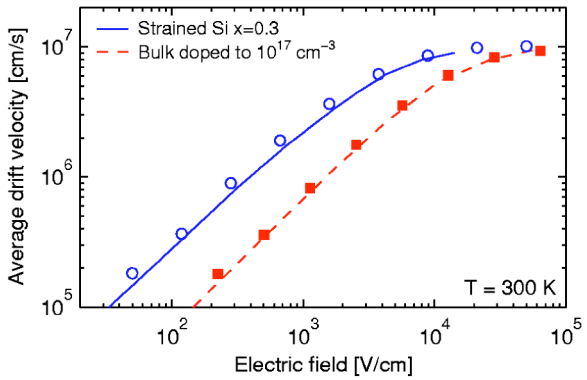

FIG. 1. Electron velocity-field relationship in bulk and strained silicon. The dashed lines represent data for 10^{17} cm^{-3} doped bulk silicon, the solid lines are data for strained silicon on $x=0.3$ substrate Ge fraction (see Ref. 16). The symbols are our simulation results for the two respective cases.

single, fixed optical phonon energy.[11] Since we are interested in the details of the phonon generation spectrum, we treat scattering with all phonon modes individually. Each branch of the dispersion is modeled with the analytic approximation $\omega_q=\omega_o+v_sq+cq_9^2$, where ω_q is the phonon frequency and q the wave vector.[9] The continuous (longitudinal) and dashed (transverse) lines in Fig. 2(a) represent this quadratic model, and the fitting coefficients are listed in Table I. Our dispersion model is otherwise assumed isotropic, since complex *ab initio* studies have shown that the anisotropic effect of the phonon dispersion is rather small.[12]

The simulation treats all phonon scattering events as inelastic, and electrons exchange energy with the lattice as determined by the phonon dispersion and scattering selection rules. Scattering with intravalley LA and TA phonons, as well as with intervalley longitudinal (LO) and transverse optical (TO) phonons, is considered individually. The phonon dispersion is also used when computing the final electron state after scattering, taking into account both momentum and energy conservation. This allows a range of phonon wave vectors and energies *around* the six typical *f*- and *g*-type phonons to participate in scattering.[9] During the simulation all phonons absorbed and emitted are tallied, and full phonon generation statistics can be computed. Figure 2 shows the computed generation spectrum in 10^{17} cm^{-3} doped bulk and strained silicon with both a lower (5 kV/cm) and higher (50 kV/cm) applied electric field. The strained silicon mobility enhancement is maintained at the lower field value, but not at the higher field, as in Fig. 1. To facilitate comparison, Fig. 2 subplots (b)–(e) are drawn such that the vertical axes with energy units in meV match the vertical frequency axis of the phonon dispersion in subplot (a) with units in rad/s, as given by $E=\hbar\omega_q$. Note the cutoff energies of the various emitted phonon populations as required by their respective dispersion relation. Few acoustic phonons are generated through intra-valley scattering at low energies because their density of states vanishes near the Brillouin zone (BZ) center. Intra-valley emission also decreases at higher energies (higher wave vectors) since fewer electrons with large enough momentum are available to emit phonons of larger wave vector.

TABLE I. Quadratic phonon dispersion coefficients.

	ω_o (10^{13} rad/s)	v_s (10^5 cm/s)	c (10^{-3} cm^2/s)
LA	0.00	9.01	−2.00
TA	0.00	5.23	−2.26
LO	9.88	0.00	−1.60
TO	10.20	−2.57	1.11

The sharp peaks in the phonon generation plots occur due to intervalley scattering with the three *g*-type (TA, LA and LO, at 0.3 of the distance to the edge of the BZ) and three *f*-type (TA, LA /LO and TO, at the edge of the BZ) phonons. The relative magnitude of the peaks depends on the choice of intervalley deformation potentials, which have been carefully calibrated.[9] Note the difference in the phonon emission spectrum between strained and bulk silicon at low electric fields, as in Figs. 2(b) and 2(c). The strain-induced band splitting suppresses *f*-type phonon emission between the two lower and four upper valleys. However, since most conduction electrons in strained silicon are confined to the

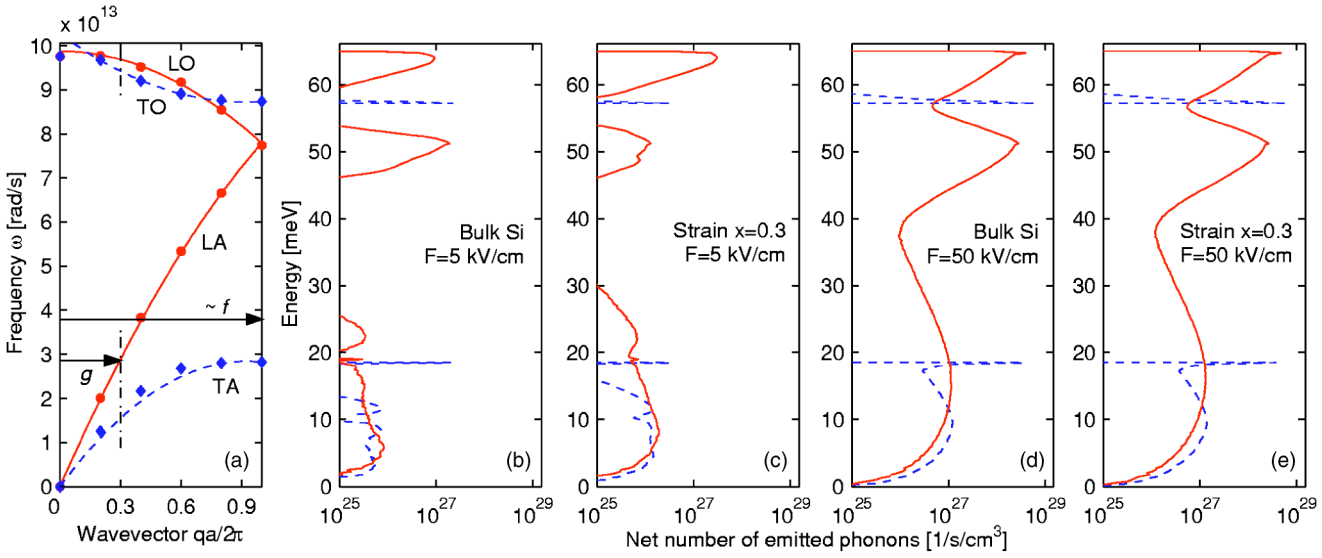

FIG. 2. Phonon dispersion in silicon (a) and computed net phonon generation rates (emission minus absorption) with low field [(b),(c)] and high field [(d),(e)] in strained and bulk silicon doped to 10^{17} cm^{-3}, at $T=300$ K. Subplot (a) shows the dispersion data of Ref. 17 (symbols), our quadratic approximation (lines), and the vector magnitude of *f*- and *g*-type intervalley phonons. Dashed lines represent transverse, while solid lines represent longitudinal phonons throughout.

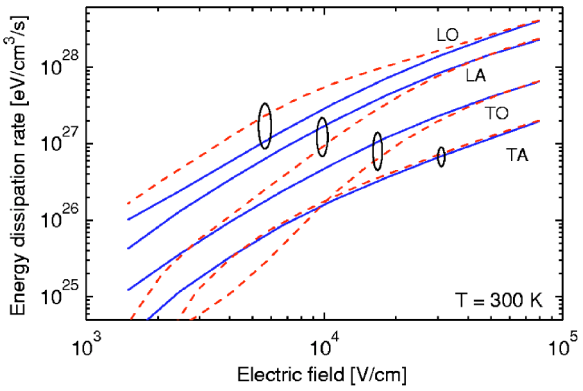

FIG. 3. Heat generation rates per phonon mode as a function of electric field. Dashed lines are for strained silicon ($x=0.3$), solid lines are for bulk silicon, both doped to 10^{17} cm^{-3}.

two lower valleys (of lighter mass m_t), they quickly gain energy and g-type emission between the lower valleys is enhanced. Comparing Figs. 2(d) and 2(e), the phonon emission spectrum in strained and bulk silicon at high field is essentially identical, an electrons have enough energy to emit across the entire phonon spectrum despite the strain-induced band splitting. This is consistent with the observation of similar saturation velocity in strained and bulk silicon (Fig. 1).

Figure 3 compares the integrated net energy dissipation rates with each branch of the phonon spectrum, at various steady-state electric fields. Note the enhancement of g-type LO emission and the reduction in energy relaxation through f-type LA and TO phonons in strained silicon. For both strained and bulk silicon the total Joule heat dissipated to the lattice, over all four phonon branches, sums up to $J \cdot E = qn\bar{v}E$ as anticipated, where J is the current density, E the electric field, q the elementary charge, n the electron density and $\bar{v}$ the average drift velocity. Emission of LO modes makes up nearly 90 percent of the energy dissipated in strained silicon at low fields, but only about half the heat generation in bulk silicon at most practical electric fields. Intervalley f-type LA phonon emission accounts for about one third, and TO emission for one tenth of the heat generation rate in bulk silicon. It should be noted that f-type scattering near the 50 meV phonon energy can be satisfied both by LA and LO phonons[12] (where the branches meet), so the distinction between the two modes is somewhat arbitrary. We assign a phonon to the LA branch when $|\mathbf{q}| < |\mathbf{G}| = 2\pi/a$, and to the LO branch otherwise, where $\mathbf{G}$ is the reciprocal lattice vector and $a=5.431$ Å is the silicon lattice constant.

In summary, this work describes an efficient Monte Carlo implementation which correctly reproduces electron transport measurements in both strained and bulk (doped) silicon. The use of analytical electron bands and phonon dispersion enables computation of the heat generation spectrum. The generated phonon distributions are different in bulk and strained silicon at low fields, but essentially the same at high fields. This work advances our understanding of self-heating in silicon, and has applications to the engineering of devices that may require detailed knowledge of the heat generation spectrum. The approach can be similarly extended to other materials (e.g., germanium) or to low-dimensional structures (e.g., nanowires).

The authors acknowledge valuable discussions with M. Fischetti, C. Jungemann, U. Ravaioli, and S. Sinha. One of the authors (E.P.) acknowledges support by the SRC-IBM graduate fellowship.

[1] G. K. Wachutka, IEEE Trans. Electron Devices **9**, 1141 (1990).
[2] U. Lindefelt, J. Appl. Phys. **75**, 942 (1994).
[3] P. G. Sverdrup, Y. S. Ju, and K. E. Goodson, J. Heat Transfer **123**, 130 (2001).
[4] J. Lai, and A. Majumdar, J. Appl. Phys. **79**, 7353 (1996).
[5] Y. S. Ju, and K. E. Goodson, Appl. Phys. Lett. **74**, 3005 (1999).
[6] S. Mazumder and A. Majumdar, J. Heat Transfer **123**, 749 (2001).
[7] M. Artaki and P. J. Price, J. Appl. Phys. **65**, 1317 (1989).
[8] P. Lugli and S. M. Goodnick, Phys. Rev. Lett. **59**, 716 (1987).
[9] E. Pop, R. W. Dutton, and K. E. Goodson, J. Appl. Phys. **96**, 4998 (2004).
[10] C. Jacoboni and L. Reggiani, Rev. Mod. Phys. **55**, 645 (1983).
[11] M. V. Fischetti and S. E. Laux, Phys. Rev. B **38**, 9721 (1988).
[12] H. Mizuno, K. Taniguchi, and C. Hamaguchi, Phys. Rev. B **48**, 1512 (1993).
[13] C. Hamaguchi, *Basic Semiconductor Physics* (Springer, New York, 2001).
[14] H. Kosina, IEEE Trans. Electron Devices **46**, 1196 (1999).
[15] T. Yamada, J.-R. Zhou, H. Miyata, and D. K. Ferry, IEEE Trans. Electron Devices **41**, 1513 (1994).
[16] K. Ismail, S. Nelson, J. Chu, and B. Meyerson, Appl. Phys. Lett. **63**, 660 (1993).
[17] G. Dolling, in Symposium on Inelastic Scattering of Neutrons in Solids and Liquids (1963), pp. 37–48, Vol. 2 (IAEA, Chalkriver).